Supplementary Material: Field-Tuned Quantum Effects in a Triangular-Lattice Ising Magnet

SAMPLE SYNTHESIS AND NEUTRON SCATTERING EXPERIMENTS.

Large size $TmMgGaO_4$ single crystals were synthesized using the floating-zone technique. The heat capacity, X-ray Laue and X-ray diffraction measurements indicate the high crystallization quality of the sample (Fig. S1) [1]. The neutron diffraction measurements were carried out on the cold three axes spectrometer PANDA at the Heinz Maier-Leibnitz Zentrum, Garching, Germany [2], and the FLEXX cold triple-axis spectrometer in the BER-II reactor at Helmholtz-Zentrum Berlin, Germany [3]. For the PANDA experiment, a vertically focused PG(002) was used as a monochromator and analyzer. We fixed the final neutron energy at $E_f = 4.06$ meV, leading to an energy resolution of around 0.1 meV. In order to avoid the contamination from neutrons with higher orders, a Be filter was placed after the sample. One piece of single crystal with mass of 3 grams was aligned in the (H, K, 0) plane. A closed-cycle refrigerator equipped with a ^{3}He insert was used to reach the base temperature of 0.485 K. For the FLEXX experiment, we used a PG(002) as both the monochromator and analyzer, and the final neutron energy was fixed at $E_f = 3.5$ meV. A velocity selector installed in front of the monochromator was used to remove the higher-order neutrons. One piece of single crystal (1.7 g) was aligned in the (H, K, 0) plane for the measurement. The sample was attached to a dilution insert and put into a vertical magnet to reach the base temperature of 40 mK.

The inelastic neutron scattering measurements were performed on the cold neutron multi-chopper spectrometer LET at the Rutherford Appleton Laboratory, Didcot, UK, and the AMATERAS cold neutron disk chopper spectrometer at the Japan Proton Accelerator Research Complex [4]. For the LET experiment, the incident energies are chosen to be 6, 3.15 and 1.94 meV with energy resolutions of 0.185, 0.069 and 0.031 meV, respectively. A dilution insert was used to reach the base temperature of 0.12 K, which was equipped with a vertical magnet to provide external fields. The same pieces of single crystals with a total mass of 17.2 g were used as in Ref. 1, which were co-aligned in the (H, K, 0) plane. For the AMATERAS experiment, we choose the incident energy to be 2.6 and 5.9 meV and the corresponding energy resolutions are 0.045 and 0.155 meV,respectively. A dilution insert with a vertical magnet is used in this experiment. One piece of single crystal was aligned in the (H, K, 0) plane which could rotate around the vertical z axis. The data were analysed using the Horace-Matlab suite [5].

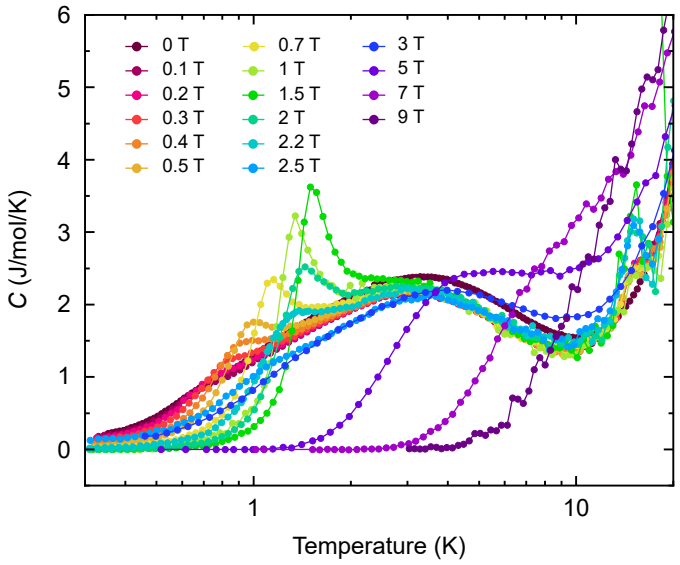

Fig. S1. Heat capacity in various longitudinal fields without phonon subtraction. The phonon subtracted data are presented in Fig. 1c.

The polarized neutron scattering experiments were carried out on the ThALES cold triple-axis spectrometer at the Institut Laue-Langevin, Grenoble, France. In this experiment, we used a focusing Heusler monochromator and analyzer to produce and analyse the polarized neutrons with the fixed final energy of $E_{\rm f} = 4.662$ meV. Longitudinal polarization analysis was done using the Helmholtz coils. A base temperature of 1.7 K is realized with this setup. One piece of single crystal with mass of ∼0.3 g was used for the measurement.

POLARIZED NEUTRON SCATTERING MEASUREMENTS.

For the polarized neutron scattering measurements, we used the conventional notations to define the polarization directions, x, y and z, in reciprocal space. To be more specific, x is defined in such a way that it keeps parallel to the momentum transfer $\mathbf{Q}$, and y is perpendicular to x but remains in the scattering plane while z is perpendicular to both x and y, thus perpendicular to the scattering plane (Fig. S2a). During the measurements, we polarized the incident neutrons along one of the basic directions, x, y or z, and selectively measured the scattered neutrons parallel or anti-parallel to the incident neutrons, which are marked as non-spin-flip (NSF) and spin-flip (SF) channels, respectively. Correspondingly, there are six different channels in total, SFx, SFy, SFz, SFx, SFy and SFz.

In the neutron scattering measurements, the neutrons are only sensitive to the magnetic components perpendicular

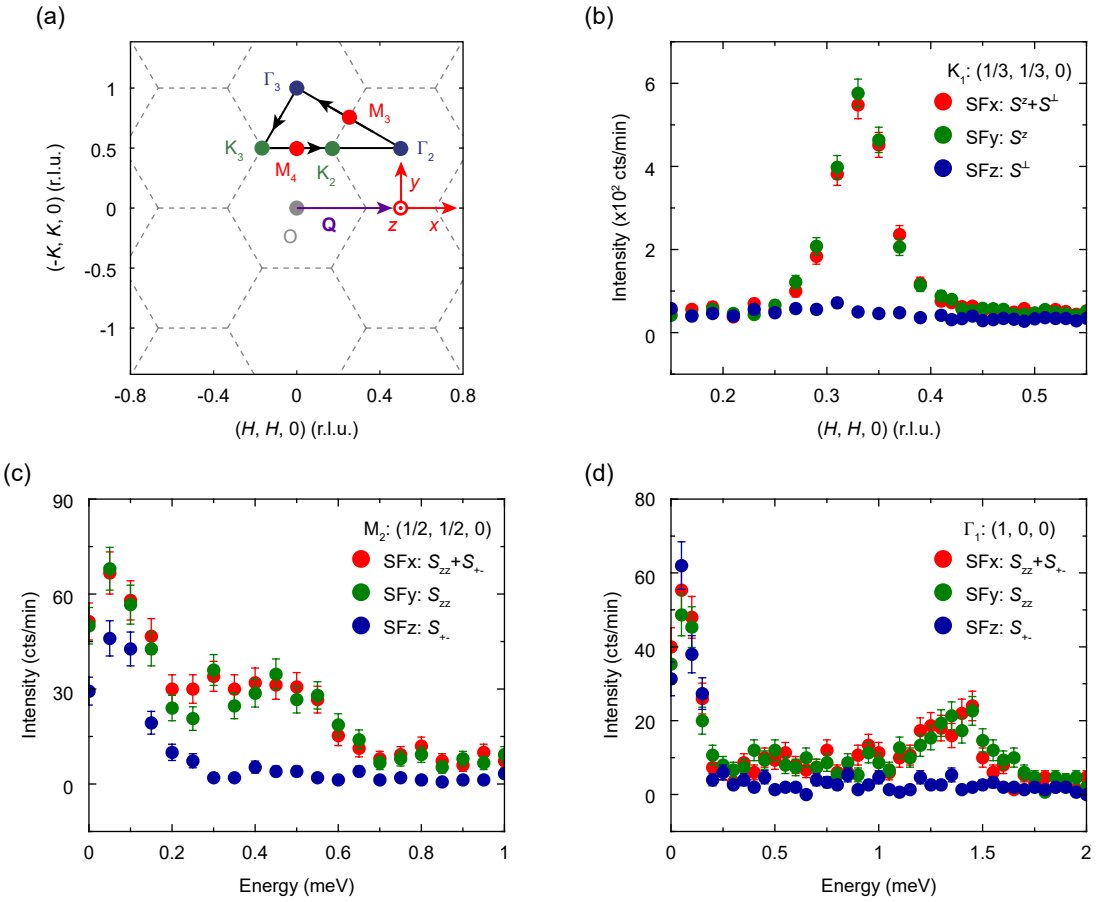

Fig. S2. Polarized neutron scattering measurements of a $TmMgGaO_4$ single crystal at 0 T and 1.7 K. (a) Sketch of the reciprocal space in the (H, K, 0) plane. The red arrows indicate the polarization directions at a representative **Q**. (b) Qscans near the magnetic Bragg peak K_1 point at $E = 0$ meV. (c),(d) Energy scans at the high symmetry points, M_2 and Γ_1.

to **Q**. Moreover, the spin of a neutron can only be flipped by magnetic components perpendicular to it with a flipping ratio determined by the instrument, leading to leakage of the signal from SF channel to NSF channel and vice versa. For elastic measurements, the scattering process probes the static spins along the z direction (S^z) or perpendicular to z ($S^\perp$) while the inelastic measurements detect the spin-spin correlations out of the basic plane (S_{zz}) and within the plane (S_{+-}). In the configuration of our experiments, the SFx channel corresponds to the components that are perpendicular to **Q**, which are S^z/S_{zz} and part of $S^\perp/S_{+-}$. Meanwhile, the SFy channel contains the components that are perpendicular to both **Q** and y, which are S^z/S_{zz} only, and the SFz channel detects the components in the xy plane but perpendicular to **Q**, which are part of $S^\perp/S_{+-}$ but no S^z/S_{zz}.

We start by the polarization analysis of the elastic signals. In Fig. S2b, we present the momentum scans across the

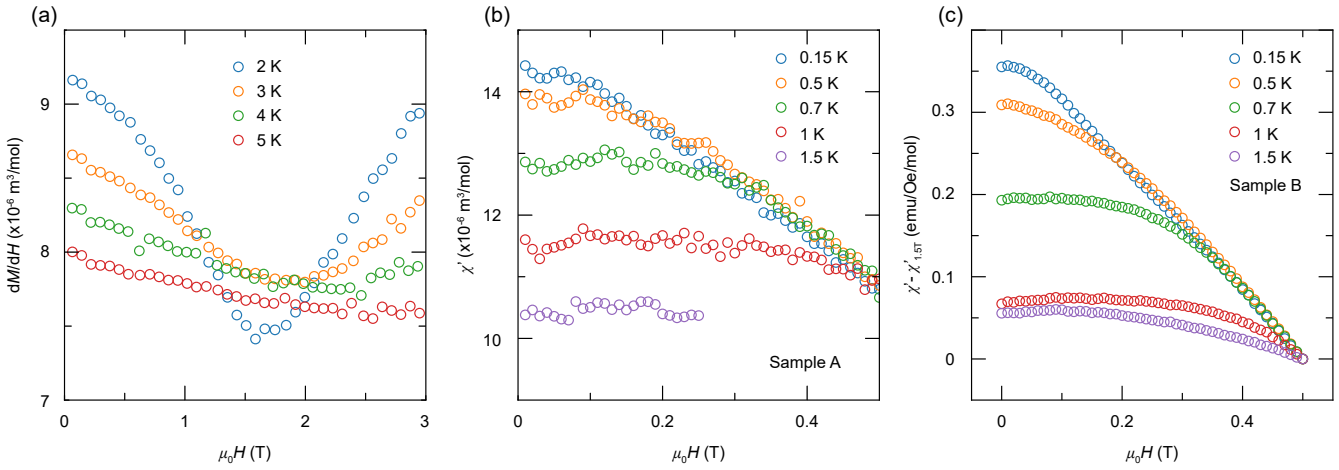

Fig. S3. Magnetic susceptibility in magnetic fields along the z axis. (a) Field dependence of the DC differential susceptibility dM/dH above 2 K. (b), (c) Real part of the ac susceptibility χ' as a function of external field at different temperatures. The measurement was performed with ac frequency of 469 Hz on two different samples. No divergence or enhancement related to the BKT phase is observed.

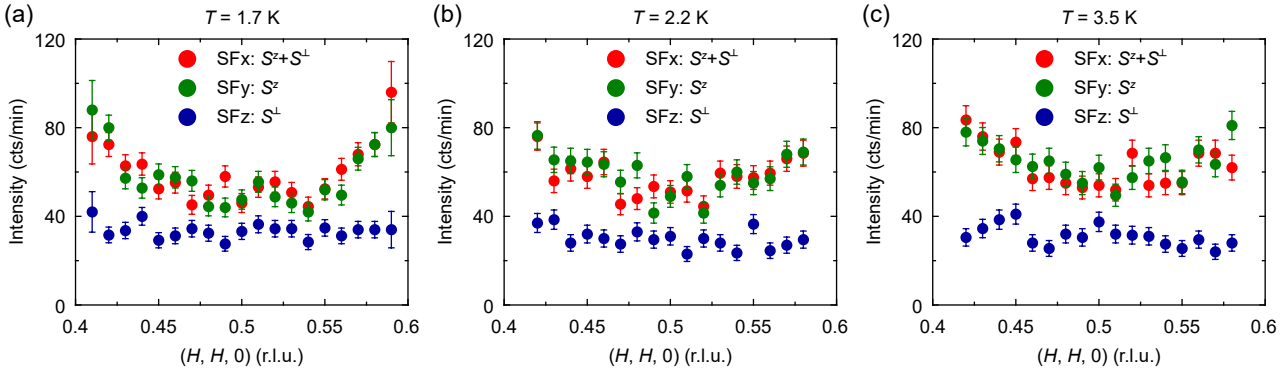

Fig. S4. Polarized neutron scattering measurements around the M_2 point at the indicated temperatures and $E = 0$ meV.

magnetic Bragg peak K_1 in all three SF channels. The measurements were performed at 1.7 K, which is above the magnetic peak saturating temperature (∼0.4 K). At this temperature range, the linewidth of the excitation spectrum is slightly broadened, but the overall spin excitation dispersion should be still similar to that observed at 0.05 K [1]. With signals absent in SFz channel, the peaks in SFx and SFy channels are comparable which means that only S^z component is observed in elastic neutron measurements, consistent with our model that the transverse $S^{\perp}$ component behaves as multipoles and cannot be detected directly. Moreover, we performed the constant **Q** scans at the high symmetry points, K_1, M_2 and Γ_1, and only magnetic excitations of S_{zz} components are present in these scans (Fig. S2c, d, Fig. 4a). The peak-like features close to the zero energy in Fig. S2c, d may come from the background or

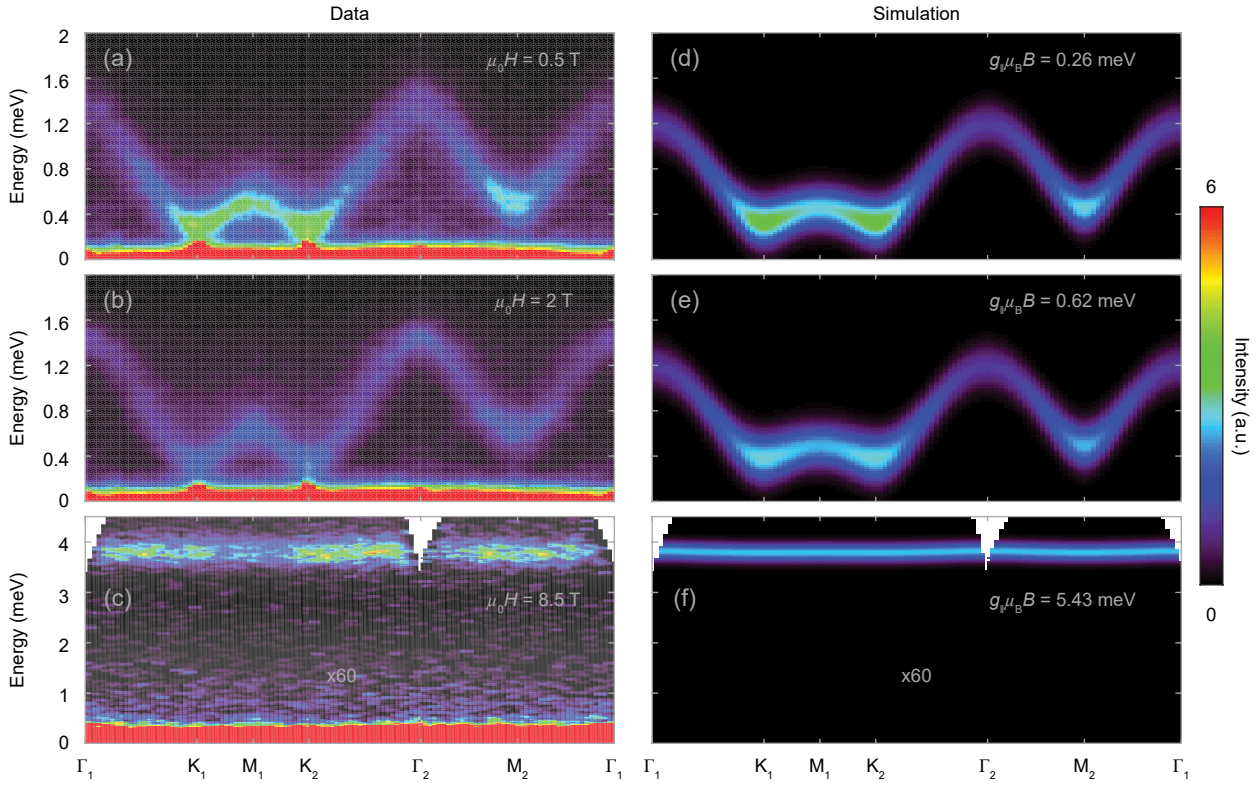

Fig. S5. Spin wave dispersion in different external longitudinal fields measured at LET and 0.12 K. (a)-(c) Spin excitations along the high symmetry reciprocal directions marked by the black arrows in Fig. 1b in the indicated fields. (c)-(f) Calculated spin wave dispersions. The intensities in (c) and (f) are multiplied by 60.

leakage since they do not obey the fundamental relationship: SFy + SFz = SFx. For conventional localized systems, the magnetic excitations run perpendicular to the static spins. Here, the spin dynamics occur in the longitudinal channels, indicating quantum effect and multipolar nature of the transverse spin components.

SUSCEPTIBILITY MEASUREMENTS.

It has been theoretically proposed that in the transverse field Ising model (TFIM) on a triangular lattice, the low-temperature three-sublattice ground state will melt in a two-step manner with an intermediate BKT phase [6–9]. In $TmMgGaO_4$. It has been predicted that the uniform susceptibility will diverge in an external field along the c direction in the BKT phase [7, 8]. According to the theoretical calculations, the susceptibility tends to diverge as $\chi(B) \sim |B|^{-[(4-18\eta)/(4-9\eta)]}$ where $\eta(T) \in (1/9, 2/9)$ (Ref. 7 and 8). To test this result, we measured the magnetic susceptibility as a function of magnetic fields and temperatures (Fig. S3). No divergence in susceptibility was observed

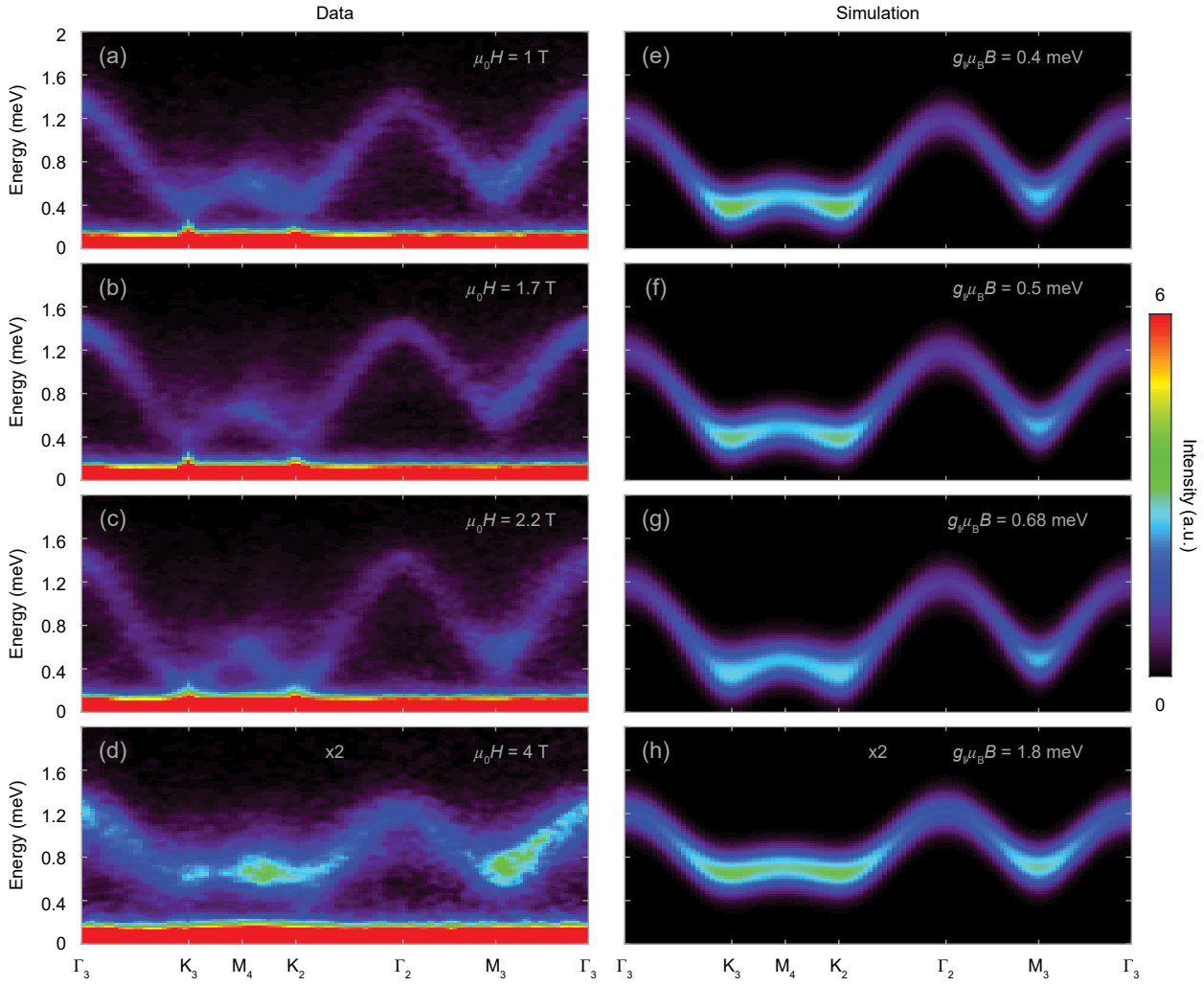

Fig. S6. Spin wave dispersion in different external fields at 0.06 K. (a)-(d) Spin excitations along the high symmetry reciprocal directions marked by the black arrows in Fig. S1a in the indicated fields. (e)-(h) Calculated spin wave dispersions. The intensities in (d) and (h) are multiplied by 2.

in the zero field limit. We note that the compressible BKT phase for the TFIM, that is characterized by a divergent correlation length and quasi-long-range order in a temperature window above the true long-range ordering transition and describes the long-distance and low-energy properties of the TFIM, is fragile to inter-layer coupling or weak disorder.

In addition, Li *et al.* suggested that there would be a magnetic peak at M points at finite temperature due to the proliferated vortex-antivortex pairs based on Monte-Carlo calculations [9]. We performed polarized elastic neutron scattering measurement across M_2 points at different temperatures and no magnetic peaks were found (Fig. S4).

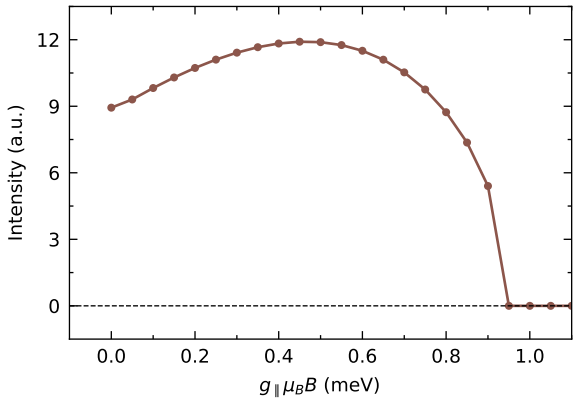

Fig. S7. Calculated field dependent evolution of magnetic Bragg peak intensity at $\mathbf{Q} = (1/3, 1/3, 0)$ using LSW.

MORE INELASTIC NEUTRON SCATTERING DATA.

The inelastic neutron scattering measurements were performed in different external longitudinal fields, 0, 0.5, 1.5, 2, 2.5, 3, 5, 8.5 T for experiments at LET and 0, 1, 1.7, 2.2, 4 T for experiments at AMATERAS. For the measurements at LET, the 8.5 T data can be taken as an ideal background since the spin gap is high enough to disentangle the low-energy background and the high-energy signals. Thus, in Fig. 4b, for the data measured between 0 and 5 T we show the background subtracted results while the raw 8.5 T data is presented. By integrating the scattering function along the energy axis, we can determine the total local moment, $\langle m^2 \rangle$, which are shown as *All* in Fig. 4c. The *elastic* contributions are evaluated by fitting the elastic lines with Gaussian profiles. The difference between the total moment and elastic channel gives the *inelastic* spectra. For the experiments at AMATERAS, no high-field data are available for background subtraction.

In the main text, we have shown the dispersion under several representative external fields (Fig. 3), along with the spin wave calculation using the SPINW program [10]. Here, we present the rest of the data, including the LET data under 0.5, 2 and 8.5 T (Fig. S5) and AMATERAS data under 1, 1.7, 2.2 and 4 T (Fig. S6). The overall dispersions are well reproduced by LSW simulations. Furthermore, we use the same approach and parameters to calculate the field dependent magnetic Bragg peak intensity at $\mathbf{Q} = (1/3, 1/3, 0)$. Only S^z is considered due to multipolar nature of S^x and S^y. As indicated by Fig. S7, the peak intensity shows a non-monotonic behavior with increasing field, consistent with our data. Due to the stronger quantum fluctuations around zero field which is not fully caught my our mean-field approach, the measured peak intensity is weaker at low field compared with calculation.

[1] Shen Y, Liu C, Qin Y, et al. Intertwined dipolar and multipolar order in the triangular-lattice magnet $TmMgGaO_4$. Nat Commun 2019;10:4530.

[2] Schneidewind A, Cermák P. PANDA: Cold three axes spectrometer. Journal of large-scale research facilities JLSRF 2015;1:12.

[3] Le M D, Quintero-Castro D L, Toft-Petersen R, et al. Gains from the upgrade of the cold neutron triple-axis spectrometer FLEXX at the BER-II reactor. Nucl Instrum Meth A 2013;729:220-226.

[4] Nakajima K, Ohira-Kawamura S, Kikuchi T, et al. AMATERAS: a cold-neutron disk chopper spectrometer. J Phys Soc Japan 2011;80:SB028.

[5] Ewings R A, Buts A, Le M D, et al. Horace: software for the analysis of data from single crystal spectroscopy experiments at time-of-flight neutron instruments. Nucl Instrum Meth A 2016;834:132-142.

[6] Isakov S V, Moessner R. Interplay of quantum and thermal fluctuations in a frustrated magnet. Phys Rev B 2003;68:104409.

[7] Damle K. Melting of three-sublattice order in easy-axis antiferromagnets on triangular and Kagome lattices. Phys Rev Lett 2015;115:127204.

[8] Biswas S, Damle K. Singular ferromagnetic susceptibility of the transverse-field Ising antiferromagnet on the triangular lattice. Phys Rev B 2018;97:085114.

[9] Li H, Liao Y D, Chen B, et al. Kosterlitz-Thouless melting of magnetic order in the triangular quantum Ising material $TmMgGaO_4$. Nat Commun 2020;11:1111.

[10] Toth S, Lake B. Linear spin wave theory for single-Q incommensurate magnetic structures. J Phys: Condens Matter 2015;27:166002.